Atmos. Chem. Phys., 24, 9263–9275, 2024
https://doi.org/10.5194/acp-24-9263-2024

Atmospheric Chemistry and Physics
Open Access
EGU

Measurement report: Formation of tropospheric brown carbon in a lifting air mass

Can Wu[1,2], Xiaodi Liu[1], Ke Zhang[1], Si Zhang[1], Cong Cao[3,4], Jianjun Li[3], Rui Li[1,2], Fan Zhang[1,2], and Gehui Wang[1,2]

[1]Key Lab of Geographic Information Science of the Ministry of Education, School of Geographic Sciences, East China Normal University, Shanghai 210062, China
[2]Institute of Eco-Chongming, 20 Cuiniao Rd., Chongming, Shanghai 202150, China
[3]State Key Laboratory of Loess and Quaternary Geology, Institute of Earth Environment, Chinese Academy of Sciences, Xi'an 710061, China
[4]School of Marine and Atmospheric Science, Stony Brook University, Stony Brook, NY 11794, USA

Correspondence: Si Zhang (szhang@geo.ecnu.edu.cn) and Gehui Wang (ghwang@geo.ecnu.edu.cn)

Received: 25 March 2024 – Discussion started: 15 April 2024
Revised: 28 June 2024 – Accepted: 9 July 2024 – Published: 26 August 2024

Abstract. An enhanced formation of brown carbon (BrC) with a non-negligible warming effect at the tropopause has recently been found. However, its formation mechanism is unclear. Here, we report on a BrC formation process that happens during air mass upward transport by conducting simultaneous measurements on atmospheric BrC with a 4 h time resolution at the mountain foot (MF, 400 m a.s.l.) and mountainside (MS, 1120 m a.s.l.) of Mt. Hua, China, in the 2016 summer. Our results showed that the daytime light absorption ($abs_{365\,nm}$) of BrC on the MS is approximately 60 % lower than that at the MF due to a dilution effect caused by the planetary boundary layer expansion, but the daytime light absorption of BrC relative to black carbon on the MS is about 30 % higher than that at the MF, suggesting a significant formation of secondary BrC in the lifting process of air mass from the MF to the MS. Such a secondary formation accounted for > 50 % of BrC on the MS but only 27 % of BrC at the MF. Moreover, the N : C elemental ratio of the daytime BrC was 15 % higher on the MS than that at the MF, mainly due to an aerosol aqueous-phase formation of water-soluble organic nitrogen (WSON) compounds. Stable nitrogen isotope composition further indicated that such light-absorbing WSON compounds were produced from the aerosol aqueous-phase reaction of carbonyls with NH_4^+. Our work revealed, for the first time, that ammonia-induced aerosol aqueous reactions can significantly promote BrC formation during the air mass lifting process, which is probably responsible for an enhanced light absorption of BrC in the upper boundary layer.

1 Introduction

Light-absorbing organic aerosols, known as brown carbon (BrC), can efficiently absorb solar radiation in the visible to near-ultraviolet (UV) wavelength range (Laskin et al., 2015; D. Liu et al., 2020; Chakrabarty et al., 2023), which corresponds to 27 %–70 % of black carbon (BC) light absorption in the lower troposphere (Saleh et al., 2015; Lin et al., 2014, 2015), suggesting that BrC can substantially perturb the planetary radiation budget (Qian et al., 2015; Lin et al., 2014; Liu et al., 2015). By absorbing solar radiation at short wavelengths, BrC can strongly alter local gas-phase photochemistry and atmospheric oxidation through decreasing the photolysis rates of OH radicals, NO_2, and O_3, leading to a reduction in atmospheric oxidant concentration of up to ∼ 30 % (Hammer et al., 2016; Gligorovski et al., 2015; Jo et al., 2016). BrC in the atmosphere also acts as a photosensitizer and produces active intermediates; thus, it can promote sulfate formation (Y. Liu et al., 2020b). In addition, BrC comprises numerous organic species and can induce adverse

human health effects because some of the chromophores are toxic (Huang et al., 2018; Hsu et al., 2014; Yan et al., 2018).

Atmospheric BrC has both primary and secondary sources. Biomass burning is believed to be the major source of primary BrC (Chakrabarty et al., 2023), while emissions from fossil fuel combustion are also an important source of primary BrC in the urban atmosphere (Yan et al., 2017; Corbin et al., 2019), which accounts for even more than 40 % of the total BrC in the heating season (Li et al., 2023). In the past decades, numerous studies have reported that BrC can also be secondarily generated in the atmosphere, such as through the photooxidation of aromatics under high NOx conditions (Lin et al., 2015; Liu et al., 2021), through NH_4^+-initiated reactions with atmospherically relevant carbonyls (Y. Li et al., 2021; Kampf et al., 2012; Laskin et al., 2014; Z. Li et al., 2019), and through OH/NO_3 radical oxidations of various volatile organic compounds (VOCs) (Sumlin et al., 2017; Gelencser et al., 2003; Lu et al., 2011). BrC is chemically active, which means it may undergo photobleaching (Schnitzler et al., 2022; Gilardoni et al., 2016), posing significant challenges for characterizing BrC molecular composition and its links to optical properties.

Recently, aircraft measurements conduced over the continental United States observed an enhanced short-wavelength optical absorption of BrC relative to BC at altitudes between 5 and 12 km (Zhang et al., 2017), indicating that secondary formation is one of the crucial sources of such high-altitude BrC. Numerical model studies reported that global radiative forcing caused by BrC ranges from 0.1 to 0.6 $W\,m^{-2}$ (Zhang et al., 2020; Lin et al., 2014; Drugé et al., 2022), suggesting a non-negligible impact of BrC on global climate change. Studies found that such climate effects are highly sensitive to BrC and that the sensitivity rapidly increases with an increase in altitude (Zhang et al., 2017; Nazarenko et al., 2017; Hodnebrog et al., 2014). The abundant BrC at the tropopause would bring about prominent impacts on radiative forcing, which could even be twice the magnitude of that induced by low-altitude BrC (Zhang et al., 2017). Due to the limited number of field observations, however, the vertical distribution and formation mechanism of tropospheric BrC are still unclear, especially in the upper troposphere, where the direct radiative forcing of BrC is much stronger than that in the ground surface atmosphere.

To elucidate the formation mechanism of BrC in the troposphere, synchronous observations on atmospheric BrC were conducted on the mountainside and at the mountain foot of Mt. Hua, which is located close to the Guanzhong basin, one of the areas with the heaviest $PM_{2.5}$ pollution in China owing to the intensive activities of fossil fuel combustion and the unfavorable topography (Q. Wang et al., 2022; Wu et al., 2020; Wang et al., 2011, 2016). Our previous study has shown that inorganic aerosol chemistry in the atmosphere over Mt. Hua is dominated by the air mass transport from the Guanzhong basin ground surface, in which $(NH_4)_2SO_4$ is continuously produced during the air mass lifting process, along with a decrease in aerosol acidity (Wu et al., 2022). Here, we investigated the formation mechanism of secondary BrC during the lifting process of air masses from the Guanzhong basin to the mountainous atmosphere of Mt. Hua. We firstly discussed the differences in the vertical distribution and optical absorption of water-soluble BrC between the ground surface and the mountainous atmosphere, and then we explored their formation mechanisms in the upper boundary layer. To the best of our knowledge, we found for the first time that ammonia-induced aerosol aqueous-phase reactions with carbonyls are the dominant formation pathway of BrC in the air mass lifting process, which is responsible for the high ratio of BrC to BC in the top troposphere.

2 Materials and methods

2.1 Sample collection

Offline $PM_{2.5}$ samples with a 4 h interval were synchronously collected onto prebaked quartz filters (at 450° for 6 h) at two locations of Mt. Hua from 27 August to 17 September 2016. One sampling site is located at the mountain foot (MF – 34°32 N, 110°5 E; 400 m a.s.l.), and another one is situated on the mountainside (MS – 34°29 N, 110°3 E; 1120 m a.s.l.) with little anthropogenic activity due to the steep terrain of the mountain region. The horizontal distance between the two sites is ∼ 8 km, and the vertical distance is about 1 km (Fig. S1 in the Supplement). As revealed in our previous study (Wu et al., 2022), vertical divergence simulated by the WRF-Chem model decreased gradually as elevation increased, along with the prevailing southerly winds, indicating the feasibility of vertical transport of air parcels from the MF to the MS. Additionally, we also note that the change in emission sources between two sites was insignificant in a lifting air mass, as indicated by the indistinctive divergences of diagnostic ratios and the proportion of organic tracers from emission sources. Such conditions can avoid the interferences caused by the emission source changes when exploring the aging process of BrC. More descriptions on the two sites have been documented in our previous study, along with the details on the sampling instrument setup (Wu et al., 2022). Mass concentrations of $PM_{2.5}$, NO_2, and O_3 at the MS site were directly quantified by E-BAM (Met One Instruments, USA) and NOx and O_3 analyzers (Thermo, Model 42i, USA; Thermo, Model 49i, USA), respectively. At the MF site, the data of the above species, apart from $PM_{2.5}$, monitored by another E-BAM, were downloaded from the Weinan Ecological Environment Bureau (http://sthjj.weinan.gov.cn/, last access: 8 July 2021). Meteorological parameters of both sampling sites were downloaded from the Shaanxi Meteorological Bureau website (http://sn.cma.gov.cn/, last access: 8 July 2021).

2.2 Chemical analysis

The organic carbon (OC) and elemental carbon (EC) of $PM_{2.5}$ filter samples were quantified by a DRI Model 2001 Thermal–Optical Carbon Analyzer following the IMPROVE-A temperature protocol (Chow et al., 2007). Water-soluble organic carbon (WSOC) and water-soluble total nitrogen (WSTN) of $PM_{2.5}$ were extracted using Milli-Q pure water (18.2 MΩ) and were determined using a total organic carbon (TOC) analyzer (Model TOC-L CPH, Shimadzu, Japan). Water-soluble organic nitrogen (WSON) is calculated by deducting the water-soluble inorganic nitrogen (WSIN) from WSTN (i.e., WSON=WSTN−WSIN). Molecular compositions (e.g., nitrophenols, polycyclic aromatic hydrocarbons – PAHs –, and other organic tracers) in the $PM_{2.5}$ filter samples were quantified by gas chromatography (HP 7890A, Agilent Co., USA) coupled with a mass spectroscopy detector (GC/MS) (HP 5975, Agilent Co., USA) after the sample extraction and derivatization. The details of the extraction and derivatization can be found elsewhere (Li et al., 2023, 2020; Wang et al., 2006). Briefly, one-fourth of the filter sample was extracted with a mixture of methanol and dichloromethane (2 : 1, v/v). Then the extracts were derivatized with N,O-bis-(trimethylsilyl) trifluoroacetamide (BSTFA).

The stable nitrogen isotope compositions of NH_4^+ ($\delta^{15}N$–NH_4^+) were determined by the isotopic analysis of nitrous oxide (N_2O) derived from the chemical conversion of NH_4^+ and were finally quantified by a PreCon–GasBench–IRMS system. This is a reliable method for nitrogen isotope analysis of the sample with a low NH_4^+ concentration, the precision of which can be up to 0.2 ‰. More details regarding the analytical artifact and quality-controlling protocols can be found in our previous studies. Furthermore, only the daytime samples were analyzed for the $\delta^{15}N$–NH_4^+ here, and a merging pretreatment was applied for the daily samples to meet the analysis requirements.

Additionally, a high-resolution time-of-flight aerosol mass spectrometer (Aerodyne Research Inc., Billerica, MA, USA) was employed to determine the chemical compositions of water-soluble organic matter (WSOM) in $PM_{2.5}$, the method of which is similar to that reported by Daellenbach et al. (2016). The offline analytical procedure has been reported previously; here, we only give a brief description (Ge et al., 2017; Sun et al., 2011). One-eighth of the $PM_{2.5}$ filter samples were extracted with pure water. Then, the water extracts were atomized using argon as the carrier gas, dried by a diffusion drier, and ultimately quantified by the aerosol mass spectrometer. Purified water was also treated in the same manner prior to each sample running, which was deemed to be an analytical blank. As we mainly focused on the WSOM chemical composition, a deep post-processing was conducted for the V-mode data in this study using the Igor-based Aerosol Mass Spectrometer Analysis Toolkit. Element ratios of WSOM, including ratios of oxygen to carbon (O/C), hydrogen to carbon (H/C), nitrogen to carbon (N/C), and organic mass to organic carbon (OM/OC), were determined according to the improved Aitken (I-A) method (Canagaratna et al., 2015). The mass load of WSOM in ambient air can be accurately estimated using Eq. (1) since the chemical species concentration in atomized aerosols depends on the flow rate of the carrier gas and extract concentration.

$$\mathrm{WSOM} = \mathrm{WSOC} \times \mathrm{OM/OC_{WSOM}} \quad (1)$$

In the above, WSOM is water-soluble organic matter (WSOM) in the atmosphere ($\mu g\,m^{-3}$); WSOC is water-soluble organic carbon (WSOC, $\mu gC\,m^{-3}$) in the atmosphere, measured by the TOC analyzer; and OM/OC_{WSOM} is the mass ratio of WSOM and OC, determined by the aerosol mass spectrometer. To obtain reliable data, the ionization efficiencies of HR-AMS were calibrated with 300 nm (D_m) ammonium nitrate and ammonium sulfate particles following the standard protocols (Sun et al., 2020; Jayne et al., 2000); furthermore, the relative ionization efficiencies (RIEs) of 4.1 and 0.8 were used for ammonium and sulfate, while the default RIEs were applied for organics, nitrate, and chloride.

2.3 Optical absorption of BrC

Measurements of the UV–Vis absorption spectra of water-soluble BrC in $PM_{2.5}$ were performed using a liquid waveguide capillary UV–Vis spectrometer with a long effective path length (1 m). The extracted solutions of BrC were prepared using a similar treatment to that used for WSOC (Sect. S1), the absorption spectra of which were converted into the absorption coefficient at a given wavelength λ (abs_λ, $M\,m^{-1}$, Eq. S1). The mass absorption efficiency (MAE_λ, $m^2\,gC^{-1}$) corresponding to water-soluble BrC at a given wavelength λ can be calculated as follows:

$$\mathrm{MAE}_\lambda = \frac{\mathrm{abs}_\lambda}{M}, \quad (2)$$

where M ($\mu gC\,m^{-3}$) is the mass concentration for water-soluble organic carbon (WSOC). The absorption Ångström exponent (AAE) indicates the spectral dependence of a species, which was quantified by a linear regression of log (abs_λ) versus log (λ) over a wavelength rang of 300–500 nm (Wu et al., 2020).

2.4 Positive matrix factorization (PMF) source apportionment

To quantitatively determine the fractional contribution of specific sources to BrC, a positive matrix factorization (PMF) receptor model (EPA PMF 5.0 version) coupled with a bootstrap technique was applied here, the principles of which have been documented in previous studies (Brinkman et al., 2006; Paatero and Tapper, 1994). Briefly, WSOC, WSON, SO_4^{2-}, NH_4^+, Mg^{2+}, Ca^{2+}, $abs_{365\,nm}$, and organic tracers

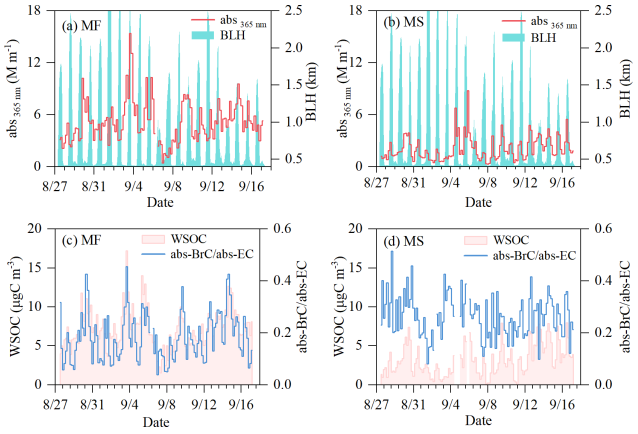

Figure 1. Temporal variations of light absorption of BrC in the ground surface (mountain foot site, MF) and the upper-boundary-layer (mountainside site, MS) atmospheres in inland China. **(a, b)** Abs_{365} and boundary layer height (BLH). **(c, d)** Concentration of WSOC and the ratio of light absorption of BrC at $\lambda = 365$ nm to BC at $\lambda = 550$ nm.

(BbF, BghiP, and levo.) are the input variables in the present work, all of which are regarded to be strong variables, expect for BghiP, with a low S/N ratio (0.6). Another input dataset is the uncertainty matrix that is calculated according to the equations outlined below (Eq. 3). The uncertainties of each factor profile are also evaluated by a bootstrap analysis, the results of which showed that the reproducibility of each source factor was > 80 % (Table S1), indicating good robustness. In our previous study on Mt. Hua (Wu et al., 2022), insignificant changes in the corresponding emission sources were revealed during the air mass lifting process. Thus, the daytime samples from both sites were added together as one data matrix. Considering Q values and interpretability, four factors were obtained as the optimal solution after numerous testes with three to seven factors, and the input species matched well with the simulated ones, with significant correlations ($R^2 > 0.88$).

$$\text{Uncertainty} = \begin{cases} \frac{5}{6} \times \text{MDL}(\text{concentration} < \text{MDL}) \\ \sqrt{(\text{error fraction} \times \text{concentration})^2 + (0.5 \times \text{MDL})^2}(\text{concentration} > \text{MDL}) \end{cases} \quad (3)$$

In the above, MDL is the method detection limit, and the error fraction is set to 5 % for $PM_{2.5}$ (Gao et al., 2018); WSOC, WSON, SO_4^{2-}, NH_4^+, Mg^{2+}, and Ca^{2+} are estimated to be 7 %, while the error fraction for the remaining species is 12 %. To reduce the error, the sample with missing data for individual species would be excluded rather than replaced by the mean value of the whole campaign.

2.5 Random forest analysis for WSON

Random forest (RF) analysis, as a powerful tool, has been used widely in regression and prediction problems regarding atmospheric pollutants; even the data have complex nonlinear relationships and interactions (Hu et al., 2017; Vu et al., 2019). To reveal the key factors that may affect the WSON formation during the air mass lifting process, an RF regression model was applied for the daytime samples at the MF and MS sites. Additionally, the potential factors herein, including pH, aerosol liquid-water content (ALWC), T, RH, NH_4^+, NH_3(aq), NO_2, nitrophenols, O_3, and organic matter (OM), were regarded to be the predictors for WSON. In the RF model design, about 70 % of these original data were randomly divided into the training dataset to construct the RF model, and the rest were deemed to be the testing data for testing the model performance. There are two important parameters that are constantly being optimized in the model construction process, namely the number of trees grown (n_{tree}) and the number of variables split at each node (n_{mtry}). After numerous tests, n_{tree} and n_{mtry} were set to be 100 and 10 for MF data and 128 and 9 for MS data to achieve the best prediction accuracy. Furthermore, a 10-fold cross-validation technique was employed here to simultaneously tune model parameters and estimate model performance. Additionally, the statistical metrics, including the coefficient of determination (R^2), mean square error (MSE) or root-mean-square error (RMSE), and mean absolute error (MAE), were established to evaluate the prediction accuracy of the model. As shown in Table S2, the predicted data for the testing dataset have strong correlativity with observation data, with small values for those error metrics. These results indicated a satisfactory performance of the RF model in explaining the importance of these factors to daytime WSON formation.

3 Results and discussion

3.1 Enhanced light absorption of BrC in the mountainous atmosphere

Figure 1 shows the temporal variations in light absorption ($abs_{365\,nm}$) and the concentrations of fine particulate WSOC simultaneously observed at the mountain foot (MF) and mountainside (MS) sites. The variation patterns of water-soluble BrC (i.e., $abs_{365\,nm}$) at both sites were closely followed by WSOC ($R^2 > 0.70$, Figs. 1 and S2); this indicated that BrC is an important part of WSOC, with the light absorption of BrC markedly increasing with decreases in light wavelengths. As summarized in Table 1, the averaged $abs_{365\,nm}$ of BrC was $2.1 \pm 1.4\,M\,m^{-1}$ on the MS, approximately corresponding to 40 % of that ($5.1 \pm 2.4\,M\,m^{-1}$) at the MF. The light absorbance level of BrC at the high-altitude MS site is in the same range as those reported from Chinese megacities such as Beijing (Cheng et al., 2016) and Xi'an (Wu et al., 2020), indicating a strong light absorption of BrC in the upper boundary layer over the Guanzhong basin of inland China. The absorption Ångström exponent (AAE) on the MS is 5.7 ± 1.3 (Table 1), slightly lower than that at the ground MF site (6.0 ± 0.5). Such a difference in AAE ($p <$

0.05) is most likely related to the difference in the chemical composition of the chromophores between the two sites with different altitudes. The averaged mass absorption efficiency (MAE) on the MS ($MAE_{365\,nm}$, $0.67 \pm 0.2\ m^2\ gC^{-1}$) was almost equal to that at the MF ($0.69 \pm 0.2\ m^2\ gC^{-1}$) but 30 %–40 % higher than those observed in Chinese megacities such as Beijing (Du et al., 2014) and Nanjing (Chen et al., 2018) ($\sim 0.5\ m^2\ gC^{-1}$ in summertime), further demonstrating the strong light absorption nature of BrC in the upper boundary layer of the Guanzhong basin of inland China.

Figure 2 shows the diurnal variations in $abs_{365\,nm}$ and $MAE_{365\,nm}$ at both sites during the campaign. At the MF site, a morning peak of $abs_{365\,nm}$ driven by enhanced traffic emissions occurred at 08:00–12:00 (local time throughout) and then gradually decreased and reached a minimum at 12:00–16:00, with the lowest MAE at 365 nm wavelength ($MAE_{365\,nm}$, $0.57 \pm 0.14\ m^2\ gC^{-1}$) (Fig. 2a and b). Such a ground surface decease in the light absorption of BrC in the early afternoon can be attributed to the daytime boundary layer growth and photobleaching. This can be verified by the oxidation state of carbon (OSc) measured by the aerosol mass spectrometer, a higher value of which is indicative of a deeper degree of atmospheric oxidation (J. J. Li et al., 2019a). As seen in Fig. 3a, $abs_{365\,nm}$ is negatively correlated with OSc, which is consistent with reported results of previous laboratory experiments (Lee et al., 2014; Zhao et al., 2015; Sumlin et al., 2017) and suggests that atmospheric aging can significantly diminish the light absorption of BrC. On the contrary, $abs_{365\,nm}$ at the MS site was remarkably enhanced with boundary layer growth and peaked at 12:00–16:00 (Fig. 2a) despite the fact that the aerosol was further oxidized during the upward transport, as indicated by the higher OSc value at the MS site (Fig. 3b). The OSc variation between both sites coincided with that of BaP/BeP, being a known proxy of whether aerosols are freshly emitted (> 1) or aged (< 1) (Fig. S3). Moreover, a moderately increased $MAE_{365\,nm}$ was also observed in this process (Fig. 2b). As shown in Table 1, the light absorption of BrC at 365 nm relative to BC at 550 nm ($abs_{365\,nm}$-BrC and $abs_{550\,nm}$-BC) during the daytime on the MS was 0.28 ± 0.08, which is approximately 30 % higher than that at the MF (0.22 ± 0.08, Table 1). Our previous study at Mt. Hua found that changes in the sources of primary organic aerosols in the air masses transported from the MF to the MS were insignificant (Wu et al., 2022), indicating that there was no additional emission of BrC during the air mass upward transport. Thus, the enhanced light absorption of BrC relative to BC on the MS is solely ascribed to a secondary formation of absorbing BrC (Fig. 2c); the secondary BrC was highly light absorbing despite being more aged atmosphere aloft, as verified by a strongly positive correlation between $MAE_{365\,nm}$ and OSc values at the MS site (Fig. S4).

To further elucidate the above hypothesis, a PMF analysis was applied for the source apportionment of the daytime $abs_{365\,nm}$ at both sites. As seen in Fig. S5, four types of

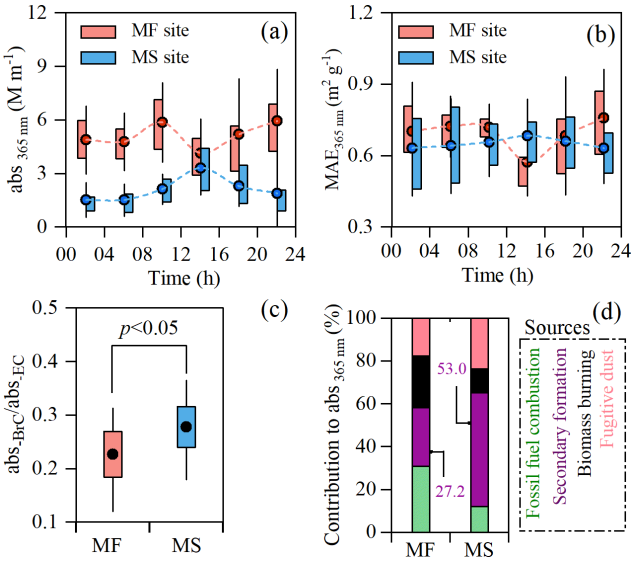

Figure 2. BrC formation in air mass lifting process. Panels **(a)** and **(b)** show the diurnal variations in $abs_{365\,nm}$ and $MAE_{365\,nm}$ at the mountain foot (MF) and mountainside (MS) sites. **(c)** Ratio of light absorption of BrC at $\lambda = 365$ nm to that of BC at $\lambda = 550$ nm ($abs_{365\,nm}$-BrC/$abs_{550\,nm}$-BC) during the daytime at both sites (the abs-BC at $\lambda = 550$ nm was calculated according to the mass absorption efficiency of EC reported by Bosch et al. (2014)). **(d)** Source apportionment for the daytime BrC at the two sites. The whisker boxes show the mean (dot), 25th–75th percentile ranges (box), and standard deviation values (whiskers).

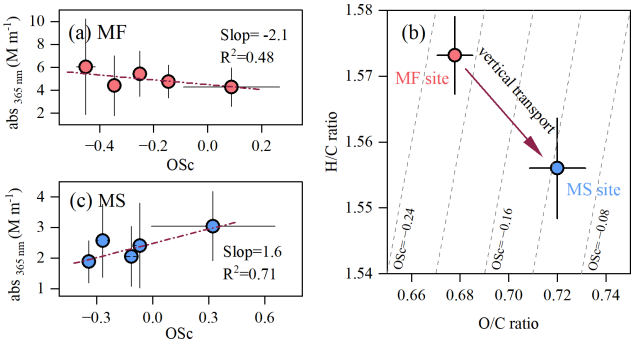

Figure 3. Evolution of chemical composition of daytime water-soluble BrC in the air mass transport from the mountain foot (MF site, red dots) to the mountainside (MS site, blue dots). Panels **(a)** and **(c)** show the light absorption ($abs_{365\,nm}$) of daytime water-soluble BrC as a function of their oxidation state (OSc=2O/C−H/C) at the MF and MS sites, respectively. **(b)** The VK triangle diagram of water-soluble BrC at the two sites.

BrC sources were identified. In brief, fossil fuel combustion and biomass burning influenced by locally related emissions were primary sources for the surface BrC, which is consistent with observations made in other cities (Li et al., 2023; Wu et al., 2020; D. Wang et al., 2022). However, BrC at the MS site was produced dominantly from secondary formation, the

Table 1. Optical properties of BrC, mass concentrations of organic carbon and nitrogen in $PM_{2.5}$, and meteorological parameters at the two sampling sites.

	Mountain foot (MF)			Mountainside (MS)		
	Average	Daytime	Nighttime	Average	Daytime	Nighttime
(i) Optical properties of BrC and acidity of $PM_{2.5}$						
abs_{365} ($M\,m^{-1}$)	5.1 ± 2.4	5.0 ± 2.5	5.2 ± 2.2	2.1 ± 1.4	2.6 ± 1.3	1.6 ± 1.3
MAE_{365} ($m^2\,gC^{-1}$)	0.69 ± 0.2	0.66 ± 0.18	0.73 ± 0.18	0.67 ± 0.21	0.67 ± 0.15	0.68 ± 0.26
AAE	6.0 ± 0.5	6.1 ± 0.51	6.0 ± 0.51	5.7 ± 1.3	5.5 ± 0.9	5.8 ± 1.7
$abs_{365\,nm}$-BrC/$abs_{550\,nm}$-BC[a]	0.18 ± 0.09	0.22 ± 0.08	0.17 ± 0.09	0.26 ± 0.08	0.28 ± 0.08	0.25 ± 0.07
pH	2.9 ± 2.0	2.3 ± 1.6	3.6 ± 2.1	3.4 ± 2.2	3.5 ± 2.2	3.3 ± 2.2
(ii) Concentrations of carbonaceous $PM_{2.5}$ and aerosol liquid-water content (ALWC)						
WSOC ($\mu gC\,m^{-3}$)	7.3 ± 2.5	7.6 ± 2.8	7.0 ± 2.1	3.2 ± 2.1	4.0 ± 2.1	2.4 ± 1.7
WSON ($\mu gN\,m^{-3}$)	2.3 ± 1.6	2.5 ± 1.7	2.0 ± 1.4	1.2 ± 0.9	1.5 ± 1.1	0.8 ± 0.7
OC ($\mu gC\,m^{-3}$)	14.0 ± 4.7	12.4 ± 4.6	15.4 ± 4.4	5.0 ± 2.8	6.3 ± 2.8	3.8 ± 2.3
EC ($\mu gC\,m^{-3}$)	4.3 ± 2.0	3.1 ± 1.0	5.4 ± 1.9	1.1 ± 0.7	1.3 ± 0.7	0.8 ± 0.4
Nitrophenols ($ng\,m^{-3}$)	16 ± 13	12 ± 10	19 ± 15	2.5 ± 1.9	3.2 ± 2.2	1.7 ± 1.1
ALWC ($\mu g\,m^{-3}$)	28 ± 64	11 ± 15	44 ± 86	27 ± 71	18 ± 24	35 ± 95
WSOC/OC	0.54 ± 0.15	0.62 ± 0.13	0.47 ± 0.11	0.62 ± 0.21	0.62 ± 0.16	0.61 ± 0.25
(iii) Meteorological parameters						
T (°)	23 ± 4.2	27 ± 3.0	20 ± 2.4	15 ± 2.5	16 ± 2.3	14 ± 2.3
RH (%)	69 ± 18	56 ± 14	81 ± 14	63 ± 20	62 ± 19	63 ± 21
Wind speed ($m\,s^{-1}$)	1.3 ± 1.1	1.5 ± 0.93	1.2 ± 1.2	3.2 ± 2.0	2.7 ± 1.5	3.8 ± 2.3
Visibility (km)	14 ± 9.5	16 ± 9.6	12 ± 9.0	22 ± 12.1	21 ± 12	24 ± 12.0

[a] The $abs_{550\,nm}$-BC was calculated according to the mass absorption efficiency (MAE) of BC (black carbon) reported by Bosch et al. (2014); the light wavelengths for the $abs_{365\,nm}$-BrC and $abs_{550\,nm}$-BC are 365 and 550 nm, respectively.

contribution of which to the total BrC is 53 % and about twice that at the MF (Fig. 2d), further corroborating a substantial formation of BrC with relatively stronger light absorptivity during the air mass lifting process. These secondarily formed BrC chromophores engender more light absorption of high-altitude BrC compared with that of BC (or EC, Fig. 2c). A similar vertical profile of BrC in the upper troposphere (5–12 km) of the continental US was also observed by in situ aircraft measurements (Zhang et al., 2017).

3.2 Secondary formation of BrC in the air mass lifting process

Figure 4a illustrates the diurnal cycles of the N : C ratio of the water-soluble organic matter in $PM_{2.5}$ measured by the high-resolution time-of-flight aerosol mass spectrometer. At the MF site, the N : C ratio did not vary much with time and even leveled off in the daytime, which indicates that the compositions of light-absorbing chromophores are similar throughout the day. Nonetheless, the diurnal pattern of the N : C ratio on the MS was analogous to that of $abs_{365\,nm}$ and $MAE_{365\,nm}$, with a daily peak at 12:00–16:00, and a moderate positive correlation was also observed between the N : C ratio and $abs_{365\,nm}$ ($R^2 = 0.38$, $P < 0.01$), suggesting that nitrogen-containing organic compounds (NOCs) make significant contributions to the BrC light absorption in the upper boundary layer. Such a result is consistent with the laboratory simulation, in which NOCs were reported to contribute up to 60 % of the absorbance of secondary BrC over a wavelength range of 300–400 nm (Lin et al., 2015). Moreover, the daytime N : C ratios were 20 % higher on the MS (0.066 ± 0.014) than those at the MF (Fig. 4a), indicating that additional NOCs were produced in the air mass lifting process. In fact, numerous N-containing organic fragments, including C_xH_yN and $C_xH_yO_zN$ at the MS site, were detected by the aerosol mass spectrometer, accounting for ~ 13 % of the total water-soluble OM. Additionally, the fractional contribution of the above fragments on the MS was enhanced by approximately 10 % compared to that at the MF site, reaching up to ~ 25 % during the day with low $PM_{2.5}$ load ($< 75\,\mu g\,m^{-3}$) (Fig. S6). This suggested an enhanced formation of WSON during the air mass transport from the lower mountain foot site to the upper mountainside site. Since WSON on the MS moderately was positively correlated with light absorption of BrC at $\lambda = 365$ nm (Fig. S7, $R^2 = 0.45$, $p < 0.05$), the enhancement in BrC light absorption on the MS can largely be attributed to secondary formation of NOCs during the air mass transport from the ground surface to the upper boundary layer.

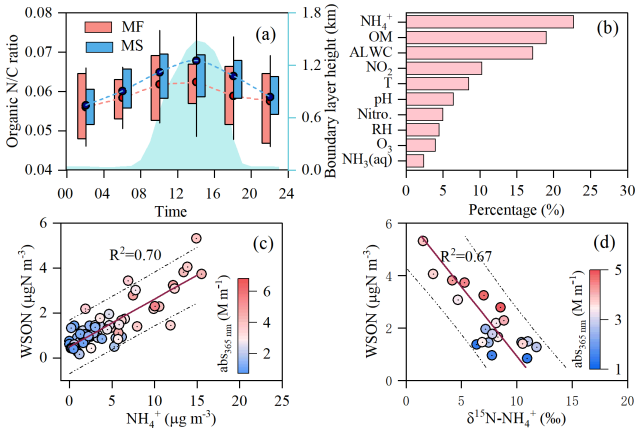

Figure 4. Formation of water-soluble organic nitrogen compounds (WSONs) in the air mass lifting process. **(a)** Diurnal variations in elemental ratio of N/C of fine particulate water-soluble organics at the mountain foot (MF) and mountainside (MS) sites; the whisker boxes show the mean (dot), 25th–75th percentile ranges (box), and standard deviation values (whiskers). **(b)** Importance assessment for the key factors affecting the daytime WSON at the MS site. Panels **(c)** and **(d)** show the linear fit regressions for WSONs with NH_4^+ and $\delta^{15}N$–NH_4^+ in the daytime $PM_{2.5}$ aerosols at the MS site, respectively.

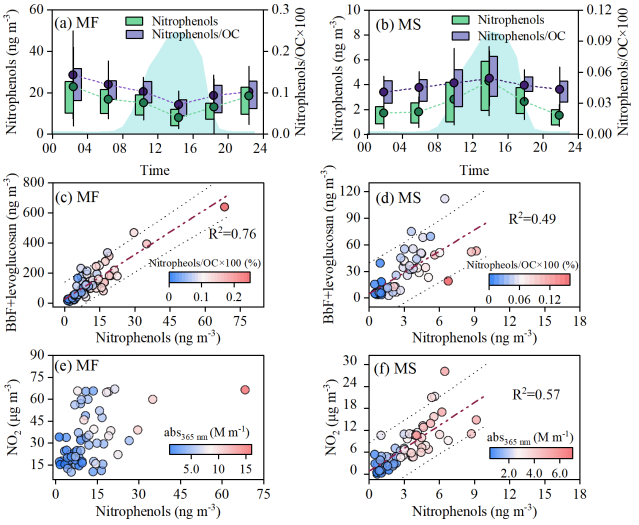

Figure 5. The source and secondary formation of nitrophenols at the MF and MS sites. **(a, b)** Diurnal variations in nitrophenols and mass ratio of nitrophenols to OC (nitrophenols/OC); blue shading indicates diurnal variations of the boundary layer height, and the whisker boxes show the mean (dot), 25th–75th percentile ranges (box), and standard deviation values (whiskers). Linear fit regression for nitrophenols with BbF+levoglucosan **(c, d)** and NO_2 **(e, f)**.

Light-absorbing NOCs, including reduced nitrogen species (e.g., imidazoles and pyrazines) and oxidized ones (e.g., nitro-aromatics), can be generated via various types of gas- and particle-phase reactions, such as NH_3-mediated carbonyl-to-imine reactions, nitration of aromatic compounds, and heterogeneous reactions of •OH and NO_2^-• radicals with phenolic compounds (Moise et al., 2015; Laskin et al., 2015). The potential pathways and dominating factors for NOC formation at the MS site will be explored in the following sections.

3.3 Gas-phase formation of BrC in the air mass lifting process

Nitro-aromatic compounds (NACs) are strong light-absorbing compounds and are ubiquitous in the atmosphere. In this study, a total of six NACs in the $PM_{2.5}$ samples were detected (Table S3), exhibiting significant correlations with $abs_{365\,nm}$ at both sampling sites (Fig. S2c and d), which indicates the important impact of NACs on the aerosol light absorption. As seen in Fig. 5a, both the NAC concentration and the NAC/OC ratio decreased gradually at the MF, reaching the daily minimum at 12:00–16:00. Such an abatement in NACs was mainly attributed to the boundary layer expansion and an enhanced photooxidation (Fig. 3). Furthermore, the daytime NACs at the MF correlated well with (BbF+levoglucosan), being known as tracers for combustion emissions ($R^2 > 0.76$, Fig. 5c), but were not correlated with gaseous NO_2 (Fig. 5e), suggesting that most of the NACs at the ground surface site were directly emitted from combustion sources. This can be further verified by the strong positive correlation of NACs and CO prevailing in combustion exhausts (Fig. S8). As partial NACs at the MF site can be transported aloft by anabatic valley winds, a moderate correlation ($R^2 = 0.49$, Fig. 5d) between NACs and (BbF+levoglucosan) was observed at the MS site. However, the moderate correlation between NO_2 and NACs ($R^2 = 0.57$, $p < 0.01$, Fig. 5f) observed on the MS suggests a non-negligible formation of secondary NACs under the transport process. As revealed by previous studies, the NO_3•/•OH oxidation of phenolic volatile organics in the presence of NOx can form numerous NACs, followed by partitioning to the condensed phase (Wang and Li, 2021; X. Li et al., 2021; Finewax et al., 2018); furthermore, the photolysis of nitrite in the aerosol aqueous phase can also lead to the nitration of phenol or catechol to generated NACs (Vione et al., 2005). However, there is a poor relationship between NACs and aerosol liquid-water content (ALWC; $R^2 = 0.34$, $P > 0.05$) and particulate phenol ($R^2 < 0.1$), indicating a minor contribution of aqueous-phase formation to NACs aloft.

The preceding discussion provided reliable evidence that partial NACs could be formed by gas-phase reactions, but they only accounted for a very small fraction of OC (Fig. 5a–b), suggesting that gas-phase formation is probably not the major formation pathway of secondary NOCs during the air mass vertical transport. Further evidence for this hypothesis

was provided by a random forest (RF) analysis, which was used as a metric for the degree of correlation between these influencing factors (ALWC, pH, T, NO_2, NH_4^+, etc.) and WSON at both sampling sites (Figs. 4b and S9). As revealed by the RF model results, nitrophenols and gaseous NO_2 were important influencing factors for the daytime WSON at the MF site (Fig. S9), the importance of which was explained by up to 35 % but only up to ~ 15 % aloft (Fig. 4b), confirming a lesser importance of the gas-phase reactions for the light-absorbing-NOC formation in the vertical-transport process.

3.4 Aerosol aqueous formation of BrC in the air mass lifting process

As shown in Fig. 4b, RF analysis showed that the variation in the concentration of WSON in $PM_{2.5}$ on the MS was largely affected by NH_4^+ (23.0 %) and ALWC (17.3 %). Given a relatively strong correlation between WSON and NH_4^+ ($R^2 = 0.70$, Fig. 4c), we proposed that aqueous-phase reactions induced by ammonium constitute the major formation pathway for water-soluble NOCs on the MS. To further demonstrate such a hypothesis, we analyzed the nitrogen isotope composition (δ^{15}N–NH_4^+) of ammonium in the $PM_{2.5}$ samples at both sites, the analytical details of which have been described in our previous study (Wu et al., 2022). As seen in Fig. 4d, WSON showed a strong negative correlation with δ^{15}N–NH_4^+, probably due to the irreversible reactions involving ammonia-favored ^{15}N depletion in the particle form, as revealed by Heaton et al. (1997). In contrast, WSON at the MF presented a similar correlation with NH_4^+ as that on the MS but did not correlate with δ^{15}N–NH_4^+ (Fig. S10a and b).

Previous studies have demonstrated the importance of NH_4^+/NH_3 in the formation of light-absorbing imidazoles and N-heterocycles from the carbonyls (e.g., glyoxal (Gly) and methylglyoxal (mGly) generated from oxidation of VOCs) (Y. Li et al., 2021; Moise et al., 2015; Kampf et al., 2012; Liu et al., 2023). Figure S11 depicts a simple reaction pathway for the above aqueous reactions, in which the chromophore products contain lower amounts of O and H atoms. Such a phenomenon was found for the daytime NOCs on the MS. As shown in Fig. 6, the H/N and O/N ratios of BrC in $PM_{2.5}$ on the MS exhibited a strongly negative correlation with the N/C ratio ($R^2 = 0.92$ for H/N and $R^2 = 0.84$ for O/N). Considering the fact that Gly and mGly are abundant in the daytime atmosphere of Mt. Hua (Qi et al., 2023), the aqueous reactions of dicarbonyls with NH_4^+/NH_3 are probably the major pathway for yielding NOCs during the vertical transport.

The above aqueous reactions could also occur at the MF site, as depicted in Fig. S11, but these were insignificant compared to those at the MS site, attributable to the disparity in chemical compositions. Our previous study found that the ground surface MF aerosols were more acidic (pH = 2.9) and dominated by NH_4HSO_4, while the upper-boundary-layer MS aerosols were less acidic (pH = 3.4) and were dominated by abundant $(NH_4)_2SO_4$. Such differences in aerosol acidity and chemical composition between the two sites can favor the formation of NOCs at the MS site, as is evident from a recent experimental observation by Y. Li et al. (2021), who found that the NOC yield on the $(NH_4)_2SO_4$ seeds exposed to Gly or mGly vapor was relatively higher than that on NH_4HSO_4 seeds. Also, they found that mGly has a larger uptake coefficient on $(NH_4)_2SO_4$ particles, with a relatively higher NOC yield compared to Gly, because mGly has a stronger interfacial attraction and thus has a more efficient nucleophilic addition involving carbenium ions (Y. Li et al., 2021). Our previous study showed that the summertime atmosphere of Mt. Hua is dominated by biogenic VOCs and that the concentration of fine particulate mGly is about 5 times that of Gly (Meng et al., 2014). Such a predominance of mGly over Gly and a less acidic aerosol aqueous-aerosol phase at the MF site are favorable for the formation of light-absorbing NOCs on $(NH_4)_2SO_4$ particles, which could mainly be responsible for the enhanced light absorption of BrC at the mountainous site, with the ratio of the light absorption of BrC to BC being higher in the upper boundary layer than that in the ground surface.

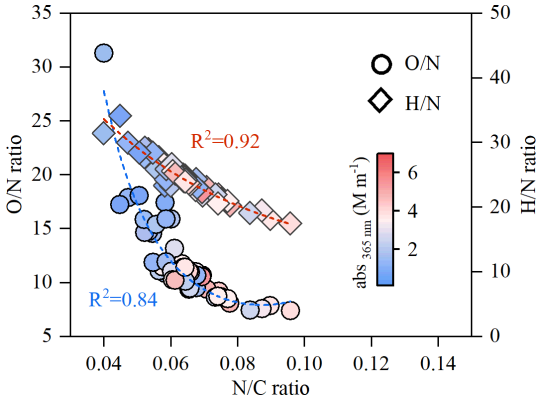

Figure 6. Elemental composition of daytime WSOC at the MS site.

3.5 Atmospheric implications

Our work provides an evolution profile of BrC during air mass vertical transport and highlights a secondary formation of BrC in this process, which could be responsible for the enhancement of BrC relative to BC in the upper boundary layer. Considering the longer lifetime of high-altitude BrC, it can disperse rapidly into a large area (Zhang et al., 2017), exerting a significant influence on regional climate that is even comparable to that of BC in the upper tropical troposphere (Jo et al., 2016). Moreover, we also revealed a vital role of aqueous-phase reactions in the secondary formation of BrC in the air mass lifting process, specifically the NH_4^+/NH_3-induced reactions (e.g., the Maillard reaction) that can form NOCs with stronger light absorptivity. As ammonia and carbonyls such as glyoxal and methylglyoxal are ubiquitous in

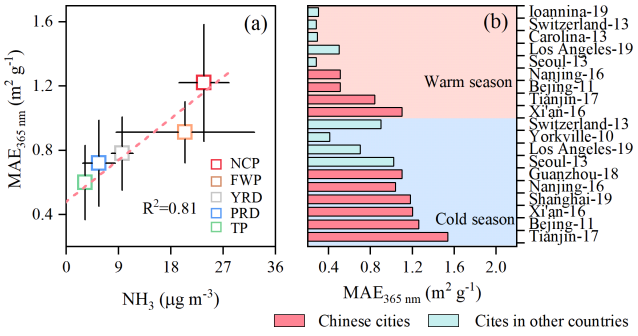

Figure 7. Impact of NH_3 on atmospheric BrC over China. **(a)** Linear correlation between NH_3 and MAE of BrC in different regions of China (NCP: North China Plain; FWP: Fenwei Plain; YRD: Yangtze River Delta; PRD: Pearl River Delta; TP: Tibetan Plain). **(b)** $MAE_{365\,nm}$ of BrC in China and other countries (the details of datasets from the literature, including specific sites, time periods, and sources, are given in Tables S4 and S5).

the troposphere, our work suggests that the above formation mechanism of the light-absorbing NOC aerosols could occur extensively in the troposphere.

In the past decade, the haze pollution in China has changed from the previous sulfate-dominated (SD) environment to the current nitrate-dominated (ND) environment due to the effective sulfur emission controls, which would significantly enhance the aerosol ALWC since nitrate is more hygroscopic than sulfate at a given RH and aerosol loading. As indicated by our previous observational evidence (Lv et al., 2023), a high ALWC load induced by abundant nitrate would efficiently promote more WSOC partitioning into aerosol phase, which may increase the BrC yield because WSOC contains numerous BrC precursors. With the increase in the relative abundance of nitrate to sulfate, nitrate-enhanced gas-to-particle partitioning of WSOC will become highly efficient in China in the near future, meaning that the BrC formation will be more active hereafter. Additionally, the national VOCs and NH_3 emissions have remained at high levels and have even shown a slight increasing trend. The abundant NH_3 not only participates in the formation of BrC but also affects BrC optical properties by regulating the aerosol acidity. To further reveal the impact on the BrC, the NH_3 concentration and $MAE_{365\,nm}$ value of water-soluble BrC in different regions of China were statistically explored on a national scale (Fig. 7a). As depicted in Fig. 7a, the spatial pattern of $MAE_{365\,nm}$ is closely coincident with NH_3 levels, with a robust positive correlation ($R^2 = 0.87$). Such a spatial distribution pattern indicates that NH_3-rich conditions are favorable for the formation of BrC with strong light absorptivity. China is one of the countries with the strongest NH_3 emissions in the world due to the huge demand for N fertilizer (Van Damme et al., 2018); thus, atmospheric NH_3 in China is much higher than that in Europe and the United States. This is probably one of the factors causing the higher concentrations of BrC with stronger light absorptivity in China compared to developed countries (Fig. 7b).

4 Conclusions

Synchronous observations of the optical properties and chemical compositions of atmospheric BrC were conducted at the MF and on the MS of Mt. Hua and revealed that the light absorption of BrC aloft was only $\sim 40\,\%$ of that at the surface owing to a dilution effect caused by planetary boundary layer upliftment. Additionally, the light absorption of BrC relative to black carbon was moderately enhanced in the lifting process of air masses from the MF to the MS, coinciding with the variation in the daytime $MAE_{365\,nm}$ aloft, indicating a secondary formation of BrC. Such secondary BrC accounted for $> 50\,\%$ of the total at the MS site, while the surface BrC mainly originated from direct combustion emissions, with a 55 % fractional contribution to the total.

The N : C ratio of WSOM was measured by offline AMS, of which the diurnal pattern was analogous to that of $abs_{365\,nm}$ and $MAE_{365\,nm}$ aloft, substantiating a considerable contribution of nitrogen-containing organic compounds (NOCs) to BrC light absorption. Furthermore, the daytime N : C ratio site was approximately 15 % higher on the MS than that at the MF, mainly due to a significant formation of secondary NOCs produced by NH_4^+/NH_3-induced reactions (e.g., the Maillard reaction). Moreover, a robust positive relationship between $MAE_{365\,nm}$ and NH_3 load was statistically explored at the national scale, show strongly that abundant NH_3 may be one of key factors for the high BrC load with strong light absorptivity in China compared to that in developed countries. Therefore, NH_3 emission control in China is indispensable for further alleviating haze and BrC pollution in the country.

Data availability. The data used in this study are freely available at https://doi.org/10.5281/zenodo.10926469 (Wu, 2024). Meteorological data and hourly $PM_{2.5}$, NO_2, and O_3 concentrations can be obtained from https://doi.org/10.5281/zenodo.7413640 (Wu, 2022).

Supplement. The supplement related to this article is available online at: https://doi.org/10.5194/acp-24-9263-2024-supplement.

Author contributions. GW designed the research and contributed the analytic tools. CW, CC, and JL collected the samples. CW, XL, KZ, and GW conducted the sample analysis. CW, SZ, and GW performed the data interpretation. CW and GW wrote the paper. All the authors contributed to the paper with useful scientific discussions.

Competing interests. The contact author has declared that none of the authors has any competing interests.

Acknowledgements. This work was financially supported by the National Natural Science Foundation of China (grant nos. 42130704 and 42007202), the National Key R&D Plan, Ministry of Science and Technology of China (grant no. 2023YFC3706302) and the ECNU Happiness Flower program.

Financial support. This research has been supported by the National Natural Science Foundation of China (grant nos. 42130704 and 42007202) and the National Key R&D Plan, Ministry of Science and Technology of China (grant no. 2023YFC3706302).

Review statement. This paper was edited by Sergey A. Nizkorodov and reviewed by three anonymous referees.

References

Bosch, C., Andersson, A., Kirillova, E. N., Budhavant, K., Tiwari, S., Praveen, P. S., Russell, L. M., Beres, N. D., Ramanathan, V., and Gustafsson, O.: Source-diagnostic dual-isotope composition and optical properties of water-soluble organic carbon and elemental carbon in the South Asian outflow intercepted over the Indian Ocean, J. Geophys. Res.-Atmos., 119, 11743–11759, https://doi.org/10.1002/2014jd022127, 2014.

Brinkman, G., Vance, G., Hannigan, M. P., and Milford, J. B.: Use of synthetic data to evaluate positive matrix factorization as a source apportionment tool for $PM_{2.5}$ exposure data, Environ. Sci. Technol., 40, 1892–1901, https://doi.org/10.1021/es051712y, 2006.

Canagaratna, M. R., Jimenez, J. L., Kroll, J. H., Chen, Q., Kessler, S. H., Massoli, P., Hildebrandt Ruiz, L., Fortner, E., Williams, L. R., Wilson, K. R., Surratt, J. D., Donahue, N. M., Jayne, J. T., and Worsnop, D. R.: Elemental ratio measurements of organic compounds using aerosol mass spectrometry: characterization, improved calibration, and implications, Atmos. Chem. Phys., 15, 253–272, https://doi.org/10.5194/acp-15-253-2015, 2015.

Chakrabarty, R. K., Shetty, N. J., Thind, A. S., Beeler, P., Sumlin, B. J., Zhang, C., Liu, P., Idrobo, J. C., Adachi, K., Wagner, N. L., Schwarz, J. P., Ahern, A., Sedlacek, A. J., Lambe, A., Daube, C., Lyu, M., Liu, C., Herndon, S., Onasch, T. B., and Mishra, R.: Shortwave absorption by wildfire smoke dominated by dark brown carbon, Nat. Geosci., 16, 683–688, https://doi.org/10.1038/s41561-023-01237-9, 2023.

Chen, Y., Ge, X., Chen, H., Xie, X., Chen, Y., Wang, J., Ye, Z., Bao, M., Zhang, Y., and Chen, M.: Seasonal light absorption properties of water-soluble brown carbon in atmospheric fine particles in Nanjing, China, Atmos. Environ., 187, 230–240, https://doi.org/10.1016/j.atmosenv.2018.06.002, 2018.

Cheng, Y., He, K.-B., Du, Z.-Y., Engling, G., Liu, J.-M., Ma, Y.-L., Zheng, M., and Weber, R. J.: The characteristics of brown carbon aerosol during winter in Beijing, Atmos. Environ., 127, 355–364, https://doi.org/10.1016/j.atmosenv.2015.12.035, 2016.

Chow, J. C., Watson, J. G., Chen, L. W. A., Chang, M. C. O., Robinson, N. F., Trimble, D., and Kohl, S.: The IMPROVE-A temperature protocol for thermal/optical carbon analysis: maintaining consistency with a long-term database, J. Air Waste Manage. Assoc., 57, 1014–1023, https://doi.org/10.3155/1047-3289.57.9.1014, 2007.

Corbin, J. C., Czech, H., Massabo, D., de Mongeot, F. B., Jakobi, G., Liu, F., Lobo, P., Mennucci, C., Mensah, A. A., Orasche, J., Pieber, S. M., Prevot, A. S. H., Stengel, B., Tay, L. L., Zanatta, M., Zimmermann, R., El Haddad, I., and Gysel, M.: Infrared-absorbing carbonaceous tar can dominate light absorption by marine-engine exhaust, npj Clim. Atmos. Sci., 2, 12, https://doi.org/10.1038/s41612-019-0069-5, 2019.

Daellenbach, K. R., Bozzetti, C., Křepelová, A., Canonaco, F., Wolf, R., Zotter, P., Fermo, P., Crippa, M., Slowik, J. G., Sosedova, Y., Zhang, Y., Huang, R.-J., Poulain, L., Szidat, S., Baltensperger, U., El Haddad, I., and Prévôt, A. S. H.: Characterization and source apportionment of organic aerosol using offline aerosol mass spectrometry, Atmos. Meas. Tech., 9, 23–39, https://doi.org/10.5194/amt-9-23-2016, 2016.

Drugé, T., Nabat, P., Mallet, M., Michou, M., Rémy, S., and Dubovik, O.: Modeling radiative and climatic effects of brown carbon aerosols with the ARPEGE-Climat global climate model, Atmos. Chem. Phys., 22, 12167–12205, https://doi.org/10.5194/acp-22-12167-2022, 2022.

Du, Z., He, K., Cheng, Y., Duan, F., Ma, Y., Liu, J., Zhang, X., Zheng, M., and Weber, R.: A yearlong study of water-soluble organic carbon in Beijing II: Light absorption properties, Atmos. Environ., 89, 235–241, https://doi.org/10.1016/j.atmosenv.2014.02.022, 2014.

Finewax, Z., de Gouw, J. A., and Ziemann, P. J.: Identification and Quantification of 4-Nitrocatechol Formed from OH and NO_3 Radical-Initiated Reactions of Catechol in Air in the Presence of NO_{ix}: Implications for Secondary Organic Aerosol Formation from Biomass Burning, Environ. Sci. Technol., 52, 1981–1989, https://doi.org/10.1021/acs.est.7b05864, 2018.

Gao, J., Wang, K., Wang, Y., Liu, S., Zhu, C., Hao, J., Liu, H., Hua, S., and Tian, H.: Temporal-spatial characteristics and source apportionment of $PM_{2.5}$ as well as its associated chemical species in the Beijing-Tianjin-Hebei region of China, Environ. Pollut., 233, 714–724, https://doi.org/10.1016/j.envpol.2017.doi:10.123, 2018.

Ge, X., Li, L., Chen, Y., Chen, H., Wu, D., Wang, J., Xie, X., Ge, S., Ye, Z., Xu, J., and Chen, M.: Aerosol characteristics and sources in Yangzhou, China resolved by offline aerosol mass spectrometry and other techniques, Environ. Pollut., 225, 74–85, https://doi.org/10.1016/j.envpol.2017.03.044, 2017.

Gelencser, A., Hoffer, A., Kiss, G., Tombacz, E., Kurdi, R., and Bencze, L.: In-situ formation of light-absorbing organic matter in cloud water, J. Atmos. Chem., 45, 25–33, https://doi.org/10.1023/a:1024060428172, 2003.

Gilardoni, S., Massoli, P., Paglione, M., Giulianelli, L., Carbone, C., Rinaldi, M., Decesari, S., Sandrini, S., Costabile, F., Gobbi, G. P., Pietrogrande, M. C., Visentin, M., Scotto, F., Fuzzi, S., and Facchini, M. C.: Direct observa-

tion of aqueous secondary organic aerosol from biomass-burning emissions, P. Natl. Acad. Sci. USA, 113, 10013–10018, https://doi.org/10.1073/pnas.1602212113, 2016.

Gligorovski, S., Strekowski, R., Barbati, S., and Vione, D.: Environmental Implications of Hydroxyl Radicals (OH), Chem. Rev., 115, 13051–13092, https://doi.org/10.1021/cr500310b, 2015.

Hammer, M. S., Martin, R. V., van Donkelaar, A., Buchard, V., Torres, O., Ridley, D. A., and Spurr, R. J. D.: Interpreting the ultraviolet aerosol index observed with the OMI satellite instrument to understand absorption by organic aerosols: implications for atmospheric oxidation and direct radiative effects, Atmos. Chem. Phys., 16, 2507–2523, https://doi.org/10.5194/acp-16-2507-2016, 2016.

Heaton, T. H. E., Spiro, B., Madeline, S., and Robertson, C.: Potential canopy influences on the isotopic composition of nitrogen and sulphur in atmospheric deposition, Oecologia, 109, 600–607, https://doi.org/10.1007/s004420050122, 1997.

Hodnebrog, O., Myhre, G., and Samset, B. H.: How shorter black carbon lifetime alters its climate effect, Nat. Commun., 5, 5065, https://doi.org/10.1038/ncomms6065, 2014.

Hsu, H.-I., Lin, M.-Y., Chen, Y.-C., Chen, W.-Y., Yoon, C., Chen, M.-R., and Tsai, P.-J.: An Integrated Approach to Assess Exposure and Health-Risk from Polycyclic Aromatic Hydrocarbons (PAHs) in a Fastener Manufacturing Industry, Int. J. Environ. Res. Pub. Health, 11, 9578–9594, https://doi.org/10.3390/ijerph110909578, 2014.

Hu, X., Belle, J. H., Meng, X., Wildani, A., Waller, L. A., Strickland, M. J., and Liu, Y.: Estimating $PM_{2.5}$ Concentrations in the Conterminous United States Using the Random Forest Approach, Environ. Sci. Technol., 51, 6936–6944, https://doi.org/10.1021/acs.est.7b01210, 2017.

Huang, R.-J., Yang, L., Cao, J., Chen, Y., Chen, Q., Li, Y., Duan, J., Zhu, C., Dai, W., Wang, K., Lin, C., Ni, H., Corbin, J. C., Wu, Y., Zhang, R., Tie, X., Hoffmann, T., O'Dowd, C., and Dusek, U.: Brown Carbon Aerosol in Urban Xi'an, Northwest China: The Composition and Light Absorption Properties, Environ. Sci. Technol., 52, 6825–6833, https://doi.org/10.1021/acs.est.8b02386, 2018.

Jayne, J. T., Leard, D. C., Zhang, X. F., Davidovits, P., Smith, K. A., Kolb, C. E., and Worsnop, D. R.: Development of an aerosol mass spectrometer for size and composition analysis of submicron particles, Aerosol Sci. Technol., 33, 49–70, https://doi.org/10.1080/027868200410840, 2000.

Jo, D. S., Park, R. J., Lee, S., Kim, S.-W., and Zhang, X.: A global simulation of brown carbon: implications for photochemistry and direct radiative effect, Atmos. Chem. Phys., 16, 3413–3432, https://doi.org/10.5194/acp-16-3413-2016, 2016.

Kampf, C. J., Jakob, R., and Hoffmann, T.: Identification and characterization of aging products in the glyoxal/ammonium sulfate system – implications for light-absorbing material in atmospheric aerosols, Atmos. Chem. Phys., 12, 6323–6333, https://doi.org/10.5194/acp-12-6323-2012, 2012.

Laskin, A., Laskin, J., and Nizkorodov, S. A.: Chemistry of Atmospheric Brown Carbon, Chem. Rev., 115, 4335–4382, https://doi.org/10.1021/cr5006167, 2015.

Laskin, J., Laskin, A., Nizkorodov, S. A., Roach, P., Eckert, P., Gilles, M. K., Wang, B., Lee, H. J., and Hu, Q.: Molecular Selectivity of Brown Carbon Chromophores, Environ. Sci. Technol., 48, 12047–12055, https://doi.org/10.1021/es503432r, 2014.

Lee, H. J., Aiona, P. K., Laskin, A., Laskin, J., and Nizkorodov, S. A.: Effect of Solar Radiation on the Optical Properties and Molecular Composition of Laboratory Proxies of Atmospheric Brown Carbon, Environ. Sci. Technol., 48, 10217–10226, https://doi.org/10.1021/es502515r, 2014.

Li, D., Wu, C., Zhang, S., Lei, Y., Lv, S., Du, W., Liu, S., Zhang, F., Liu, X., Liu, L., Meng, J., Wang, Y., Gao, J., and Wang, G.: Significant coal combustion contribution to water-soluble brown carbon during winter in Xingtai, China: Optical properties and sources, J. Environ. Sci., 124, 892–900, https://doi.org/10.1016/j.jes.2022.02.026, 2023.

Li, J., Zhang, Q., Wang, G., Li, J., Wu, C., Liu, L., Wang, J., Jiang, W., Li, L., Ho, K. F., and Cao, J.: Optical properties and molecular compositions of water-soluble and water-insoluble brown carbon (BrC) aerosols in northwest China, Atmos. Chem. Phys., 20, 4889–4904, https://doi.org/10.5194/acp-20-4889-2020, 2020.

Li, L. J., Ho, S. S. H., Feng, B., Xu, H., Wang, T., Wu, R., Huang, W., Qu, L., Wang, Q., and Cao, J.: Characterization of particulate-bound polycyclic aromatic compounds (PACs) and their oxidations in heavy polluted atmosphere: A case study in urban Beijing, China during haze events, Sci. Total Environ., 660, 1392–1402, https://doi.org/10.1016/j.scitotenv.2019.01.078, 2019a.

Li, X., Hu, M., Wang, Y., Xu, N., Fan, H., Zong, T., Wu, Z., Guo, S., Zhu, W., Chen, S., Dong, H., Zeng, L., Yu, X., and Tang, X.: Links between the optical properties and chemical compositions of brown carbon chromophores in different environments: Contributions and formation of functionalized aromatic compounds, Sci. Total Environ., 786, 147418, https://doi.org/10.1016/j.scitotenv.2021.147418, 2021a.

Li, Y., Ji, Y., Zhao, J., Wang, Y., Shi, Q., Peng, J., Wang, Y., Wang, C., Zhang, F., Wang, Y., Seinfeld, J. H., and Zhang, R.: Unexpected Oligomerization of Small alpha-Dicarbonyls for Secondary Organic Aerosol and Brown Carbon Formation, Environ. Sci. Technol., 55, 4430–4439, https://doi.org/10.1021/acs.est.0c08066, 2021b.

Li, Z., Nizkorodov, S. A., Chen, H., Lu, X., Yang, X., and Chen, J.: Nitrogen-containing secondary organic aerosol formation by acrolein reaction with ammonia/ammonium, Atmos. Chem. Phys., 19, 1343–1356, https://doi.org/10.5194/acp-19-1343-2019, 2019b.

Lin, G., Penner, J. E., Flanner, M. G., Sillman, S., Xu, L., and Zhou, C.: Radiative forcing of organic aerosol in the atmosphere and on snow: Effects of SOA and brown carbon, J. Geophys. Res.-Atmos., 119, 7453–7476, https://doi.org/10.1002/2013jd021186, 2014.

Lin, P., Liu, J., Shilling, J. E., Kathmann, S. M., Laskin, J., and Laskin, A.: Molecular characterization of brown carbon (BrC) chromophores in secondary organic aerosol generated from photo-oxidation of toluene, Phys. Chem. Chem. Phys., 17, 23312–23325, https://doi.org/10.1039/c5cp02563j, 2015.

Liu, D., He, C., Schwarz, J. P., and Wang, X.: Lifecycle of light-absorbing carbonaceous aerosols in the atmosphere, npj Clim. Atmos. Sci., 3, 40, https://doi.org/10.1038/s41612-020-00145-8, 2020.

Liu, S., Aiken, A. C., Gorkowski, K., Dubey, M. K., Cappa, C. D., Williams, L. R., Herndon, S. C., Massoli, P., Fortner, E. C., Chhabra, P. S., Brooks, W. A., Onasch, T. B., Jayne, J. T., Worsnop, D. R., China, S., Sharma, N., Mazzoleni, C.,

Xu, L., Ng, N. L., Liu, D., Allan, J. D., Lee, J. D., Fleming, Z. L., Mohr, C., Zotter, P., Szidat, S., and Prevot, A. S. H.: Enhanced light absorption by mixed source black and brown carbon particles in UK winter, Nat. Commun., 6, 8435, https://doi.org/10.1038/ncomms9435, 2015.

Liu, S., Huang, D., Wang, Y., Zhang, S., Liu, X., Wu, C., Du, W., and Wang, G.: Synergetic effects of NH_3 and NO_x on the production and optical absorption of secondary organic aerosol formation from toluene photooxidation, Atmos. Chem. Phys., 21, 17759–17773, https://doi.org/10.5194/acp-21-17759-2021, 2021.

Liu, X., Wang, H., Wang, F., Lv, S., Wu, C., Zhao, Y., Zhang, S., Liu, S., Xu, X., Lei, Y., and Wang, G.: Secondary Formation of Atmospheric Brown Carbon in China Haze: Implication for an Enhancing Role of Ammonia, Environ. Sci. Technol., 57, 11163–11172, https://doi.org/10.1021/acs.est.3c03948, 2023.

Liu, Y., Wang, T., Fang, X., Deng, Y., Cheng, H., Bacha, A.-U.-R., Nabi, I., and Zhang, L.: Brown carbon: An underlying driving force for rapid atmospheric sulfate formation and haze event, Sci. Total Environ., 734, 139415, https://doi.org/10.1016/j.scitotenv.2020.139415, 2020.

Lu, J. W., Flores, J. M., Lavi, A., Abo-Riziq, A., and Rudich, Y.: Changes in the optical properties of benzo a pyrene-coated aerosols upon heterogeneous reactions with NO_2 and NO_3, Phys. Chem. Chem. Phys., 13, 6484–6492, https://doi.org/10.1039/c0cp02114h, 2011.

Lv, S., Wu, C., Wang, F., Liu, X., Zhang, S., Chen, Y., Zhang, F., Yang, Y., Wang, H., Huang, C., Fu, Q., Duan, Y., and Wang, G.: Nitrate-Enhanced Gas-to-Particle-Phase Partitioning of Water- Soluble Organic Compounds in Chinese Urban Atmosphere: Implications for Secondary Organic Aerosol Formation, Environ. Sci. Technol. Lett., 10, 14–20, https://doi.org/10.1021/acs.estlett.2c00894, 2023.

Meng, J., Wang, G., Li, J., Cheng, C., Ren, Y., Huang, Y., Cheng, Y., Cao, J., and Zhang, T.: Seasonal characteristics of oxalic acid and related SOA in the free troposphere of Mt. Hua, central China: Implications for sources and formation mechanisms, Sci. Total Environ., 493, 1088–1097, https://doi.org/10.1016/j.scitotenv.2014.04.086, 2014.

Moise, T., Flores, J. M., and Rudich, Y.: Optical Properties of Secondary Organic Aerosols and Their Changes by Chemical Processes, Chem. Rev., 115, 4400–4439, https://doi.org/10.1021/cr5005259, 2015.

Nazarenko, L., Rind, D., Tsigaridis, K., Del Genio, A. D., Kelley, M., and Tausnev, N.: Interactive nature of climate change and aerosol forcing, J. Geophys. Res.-Atmos., 122, 3457–3480, https://doi.org/10.1002/2016jd025809, 2017.

Paatero, P. and Tapper, U.: Positive matrix factorization: A non-negative factor model with optimal utilization of error estimates of data values, Environmetrics, 5, 111–126, https://doi.org/10.1002/env.3170050203, 1994.

Qi, W. N., Zhang, Y. F., Shen, M. X., Li, L., Dai, W. T., Chen, Y. K., Liu, Y. L., Guo, X., Cao, Y., Wang, X., Jiang, Y. K., and Li, J. J.: Comparison of Gas-Particle Partitioning of Glyoxal and Methylglyoxal in the Summertime Atmosphere at the Foot and Top of Mount Hua, Molecules, 28, 5276, https://doi.org/10.3390/molecules28135276, 2023.

Qian, Y., Yasunari, T. J., Doherty, S. J., Flanner, M. G., Lau, W. K. M., Ming, J., Wang, H., Wang, M., Warren, S. G., and Zhang, R.: Light-absorbing Particles in Snow and Ice: Measurement and Modeling of Climatic and Hydrological impact, Adv. Atmos. Sci., 32, 64–91, https://doi.org/10.1007/s00376-014-0010-0, 2015.

Saleh, R., Marks, M., Heo, J., Adams, P. J., Donahue, N. M., and Robinson, A. L.: Contribution of brown carbon and lensing to the direct radiative effect of carbonaceous aerosols from biomass and biofuel burning emissions, J. Geophys. Res.-Atmos., 120, 10285–10296, https://doi.org/10.1002/2015jd023697, 2015.

Schnitzler, E. G., Gerrebos, N. G. A., Carter, T. S., Huang, Y., Healdc, C. L., Bertram, A. K., and Abbatt, J. P. D.: Rate of atmospheric brown carbon whitening governed by environmental conditions, P. Natl. Acad. Sci. USA, 119, e2205610119, https://doi.org/10.1073/pnas.2205610119, 2022.

Sumlin, B. J., Pandey, A., Walker, M. J., Pattison, R. S., Williams, B. J., and Chakrabarty, R. K.: Atmospheric Photooxidation Diminishes Light Absorption by Primary Brown Carbon Aerosol from Biomass Burning, Environ. Sci. Technol. Lett., 4, 540–545, https://doi.org/10.1021/acs.estlett.7b00393, 2017.

Sun, Y., Zhang, Q., Zheng, M., Ding, X., Edgerton, E. S., and Wang, X.: Characterization and Source Apportionment of Water-Soluble Organic Matter in Atmospheric Fine Particles ($PM_{2.5}$) with High-Resolution Aerosol Mass Spectrometry and GC-MS, Environ. Sci. Technol., 45, 4854–4861, https://doi.org/10.1021/es200162h, 2011.

Sun, Y., Lei, L., Zhou, W., Chen, C., He, Y., Sun, J., Li, Z., Xu, W., Wang, Q., Ji, D., Fu, P., Wang, Z., and Worsnop, D. R.: A chemical cocktail during the COVID-19 outbreak in Beijing, China: Insights from six-year aerosol particle composition measurements during the Chinese New Year holiday, Sci. Total Environ., 742, 140739, https://doi.org/10.1016/j.scitotenv.2020.140739, 2020.

Van Damme, M., Clarisse, L., Whitburn, S., Hadji-Lazaro, J., Hurtmans, D., Clerbaux, C., and Coheur, P.-F.: Industrial and agricultural ammonia point sources exposed, Nature, 564, 99–103, https://doi.org/10.1038/s41586-018-0747-1, 2018.

Vione, D., Maurino, V., Minero, C., and Pelizzetti, E.: Aqueous atmospheric chemistry: Formation of 2,4-dinitrophenol upon nitration of 2-nitrophenol and 4-nitrophenol in solution, Environ. Sci. Technol., 39, 7921–7931, https://doi.org/10.1021/es050824m, 2005.

Vu, T. V., Shi, Z., Cheng, J., Zhang, Q., He, K., Wang, S., and Harrison, R. M.: Assessing the impact of clean air action on air quality trends in Beijing using a machine learning technique, Atmos. Chem. Phys., 19, 11303–11314, https://doi.org/10.5194/acp-19-11303-2019, 2019.

Wang, D., Shen, Z., Zhang, Q., Lei, Y., Zhang, T., Huang, S., Sun, J., Xu, H., and Cao, J.: Winter brown carbon over six of China's megacities: light absorption, molecular characterization, and improved source apportionment revealed by multilayer perceptron neural network, Atmos. Chem. Phys., 22, 14893–14904, https://doi.org/10.5194/acp-22-14893-2022, 2022.

Wang, G., Li, J., Cheng, C., Hu, S., Xie, M., Gao, S., Zhou, B., Dai, W., Cao, J., and An, Z.: Observation of atmospheric aerosols at Mt. Hua and Mt. Tai in central and east China during spring 2009 – Part 1: EC, OC and inorganic ions, Atmos. Chem. Phys., 11, 4221–4235, https://doi.org/10.5194/acp-11-4221-2011, 2011.

Wang, G. H., Kawamura, K., Lee, S., Ho, K. F., and Cao, J. J.: Molecular, seasonal, and spatial distributions of organic aerosols

from fourteen Chinese cities, Environ. Sci. Technol., 40, 4619–4625, https://doi.org/10.1021/es060291x, 2006.

Wang, G. H., Zhang, R. Y., Gomez, M. E., Yang, L. X., Zamora, M. L., Hu, M., Lin, Y., Peng, J. F., Guo, S., Meng, J. J., Li, J. J., Cheng, C. L., Hu, T. F., Ren, Y. Q., Wang, Y. S., Gao, J., Cao, J. J., An, Z. S., Zhou, W. J., Li, G. H., Wang, J. Y., Tian, P. F., Marrero-Ortiz, W., Secrest, J., Du, Z. F., Zheng, J., Shang, D. J., Zeng, L. M., Shao, M., Wang, W. G., Huang, Y., Wang, Y., Zhu, Y. J., Li, Y. X., Hu, J. X., Pan, B., Cai, L., Cheng, Y. T., Ji, Y. M., Zhang, F., Rosenfeld, D., Liss, P. S., Duce, R. A., Kolb, C. E., and Molina, M. J.: Persistent sulfate formation from London Fog to Chinese haze, P. Natl. Acad. Sci. USA, 113, 13630–13635, https://doi.org/10.1073/pnas.1616540113, 2016.

Wang, Q., Zhou, Y., Ma, N., Zhu, Y., Zhao, X., Zhu, S., Tao, J., Hong, J., Wu, W., Cheng, Y., and Su, H.: Review of Brown Carbon Aerosols in China: Pollution Level, Optical Properties, and Emissions, J. Geophys. Res.-Atmos., 127, e2021JD035473, https://doi.org/10.1029/2021jd035473, 2022.

Wang, S. and Li, H.: NO_3 center dot-Initiated Gas-Phase Formation of Nitrated Phenolic Compounds in Polluted Atmosphere, Environ. Sci. Technol., 55, 2899–2907, https://doi.org/10.1021/acs.est.0c08041, 2021.

Wu, C., Cao, C., Li, J., Lv, S., Li, J., Liu, X., Zhang, S., Liu, S., Zhang, F., Meng, J., and Wang, G.: Different physicochemical behaviors of nitrate and ammonium during transport: a case study on Mt. Hua, China, Atmos. Chem. Phys., 22, 15621–15635, https://doi.org/10.5194/acp-22-15621-2022, 2022.

Wu, C., Wang, G., Li, J., Li, J., Cao, C., Ge, S., Xie, Y., Chen, J., Li, X., Xue, G., Wang, X., Zhao, Z., and Cao, F.: The characteristics of atmospheric brown carbon in Xi'an, inland China: sources, size distributions and optical properties, Atmos. Chem. Phys., 20, 2017–2030, https://doi.org/10.5194/acp-20-2017-2020, 2020.

Wu, C.: Observation of Brown carbon and its optical properties on Mt. Hua, Zenodo [data set], https://doi.org/10.5281/zenodo.10926470, 2024.

Wu, C.: Synchronous observation of aerosol at Mt. Hua, Version 1, Zenodo [data set], https://doi.org/10.5281/zenodo.7413640, 2022.

Yan, C., Zheng, M., Bosch, C., Andersson, A., Desyaterik, Y., Sullivan, A. P., Collett, J. L., Zhao, B., Wang, S., He, K., and Gustafsson, O.: Important fossil source contribution to brown carbon in Beijing during winter, Sci. Rep., 7, 43182, https://doi.org/10.1038/srep43182, 2017.

Yan, J., Wang, X., Gong, P., Wang, C., and Cong, Z.: Review of brown carbon aerosols: Recent progress and perspectives, Sci. Total Environ., 634, 1475–1485, https://doi.org/10.1016/j.scitotenv.2018.04.083, 2018.

Zhang, A., Wang, Y., Zhang, Y., Weber, R. J., Song, Y., Ke, Z., and Zou, Y.: Modeling the global radiative effect of brown carbon: a potentially larger heating source in the tropical free troposphere than black carbon, Atmos. Chem. Phys., 20, 1901–1920, https://doi.org/10.5194/acp-20-1901-2020, 2020.

Zhang, Y., Forrister, H., Liu, J., Dibb, J., Anderson, B., Schwarz, J. P., Perring, A. E., Jimenez, J. L., Campuzano-Jost, P., Wang, Y., Nenes, A., and Weber, R. J.: Top-of-atmosphere radiative forcing affected by brown carbon in the upper troposphere, Nat. Geosci., 10, 486–489, https://doi.org/10.1038/ngeo2960, 2017.

Zhao, R., Lee, A. K. Y., Huang, L., Li, X., Yang, F., and Abbatt, J. P. D.: Photochemical processing of aqueous atmospheric brown carbon, Atmos. Chem. Phys., 15, 6087–6100, https://doi.org/10.5194/acp-15-6087-2015, 2015.